

## Computational phantoms for investigating impact of noise magnitude on modulation transfer function

Choirul Anam<sup>1</sup>, Ariij Naufal<sup>1</sup>, Heri Sutanto<sup>1</sup>, Geoff Dougherty<sup>2</sup>

<sup>1</sup>Department of Physics, Faculty of Sciences and Mathematics, Diponegoro University, Semarang Indonesia

<sup>2</sup>Department of Applied Physics and Medical Imaging, California State University Channel Islands, Camarillo, United States of America

### Article Info

#### Article history:

Received Mar 30, 2021

Revised Jun 10, 2022

Accepted Jul 4, 2022

#### Keywords:

Computational phantom

Computed tomography

Image quality

Modulation transfer function

Spatial resolution

### ABSTRACT

Accurate measurement of spatial resolution in terms of modulation transfer function (MTF) is essential in computed tomography (CT) images. The purpose of this study was to develop a computational phantom that can be used to evaluate the effect of noise on the MTF in CT images. Our computational phantoms for measuring MTF in CT were developed with MATLAB software. The phantom image was blurred by a point spread function of a certain standard deviation. Subsequently, different noise levels were added to the phantoms. Next, an automatic MTF calculation was implemented. The first step of the MTF calculation was to determine the region of interest (ROI). Profile was generated from the ROI, and a line spread function (LSF) curve was formed. The LSF curve was Fourier transformed to produce a MTF curve. Greater noise added to phantom image, it yields greater effect of standard deviation on the measured MTF. The greater noise makes the MTF curve increase differently than MTF with 0 HU noise. The 10% MTF values at the 25% noise reach more than 2.0 cycle/mm. By the developed computational phantoms, the spatial resolution and the amount of noise can be determined independently.

This is an open access article under the [CC BY-SA](https://creativecommons.org/licenses/by-sa/4.0/) license.



### Corresponding Author:

Choirul Anam

Department of Physics, Faculty of Sciences and Mathematics, Diponegoro University

Street of Prof. Soedarto, SH Tembalang, Semarang 50275, Central Java, Indonesia

Email: anam@fisika.fsm.undip.ac.id

## 1. INTRODUCTION

An important parameter which directly indicates the image quality of computed tomography (CT) is spatial resolution [1]–[3]. Spatial resolution is the ability to distinguish small objects that are close to each other [4]. It is usually presented using the modulation transfer function (MTF) with a cut-off value of 10%. The measurement of spatial resolution in CT can be manually or automatically carried out on dedicated specific phantoms, such as the American Association of Physicists in Medicine (AAPM) CT performance phantoms [5], CatPhan phantoms, or American College of Radiology (ACR) phantoms [6]–[8]. MTF can be measured from several objects, including the point spread function (PSF) [9], line spread function (LSF) [10], [11] and edge spread function (ESF) [12], [13]. The precise and accurate measurement of MTF can be used to compare the effects of different scan parameters [14], [15], reconstruction filters [16], [17], field of view (FOV) [6], [18], focal spot size [19], [20], and others [21], [22].

Although there is no theoretical relationship between noise and MTF, a previous study reported that accurate and precise MTF measurements depend on the noise level in an image [23]. High noise level causes fluctuations in the MTF, and hence reduce the accuracy and precision of the MTF measurement [24]. The image noise can be from the exposure factors [25]–[27], detector noise and quantum noise [28], quantum

detection efficiency (QDE), and geometric detection efficiency [29], [30]. Hence, many studies suggested that obtaining accurate spatial resolution should be performed at a low noise level [21], [31].

There are several studies that have attempted to measure the MTF values of noisy images [23], [32]. Mori [32] introduced a fitting technique in a noisy image with low contrast resolution, which yielded the same MTF value as the theory. Takenaga *et al.* [23] also reported that MTF measurements obtained by curve-fitting produced MTF values that were resistant to noise both in high and low contrast objects. If the fitting technique was not applied, there were many peaks on the LSF, producing high MTF values at high frequency values [32].

The quantitative effect of noise on the MTF measurement in the radiograph has been shown by Gonzalez using three artificial phantoms [28]: edge, bar, and star bar phantoms. For the edge phantom, the uncertainty was  $\pm 0.036$ , for the bar phantom  $\pm 0.026$ , and for the star bar phantom  $\pm 0.026$  at a frequency of  $0.7 \text{ mm}^{-1}$  [28]. This is evidence that noise produces a large uncertainty in the MTF measurement. However, no study reported the limit of noise level for measuring accurate and precise MTF. In this paper, computational phantoms to investigate the effect of noise level on the accuracy and precision of MTF values in CT images were developed. To achieve the goal, the contrast of the wire and background objects was varied. Based on the result of this study, the limit of noise level on accuracy and precision of the MTF will be obtained.

**2. METHOD**

**2.1. Phantom design**

We developed computational phantoms using MATLAB software. The phantoms consisted of a circular object with a diameter of 512 pixels mimicking water with a value of 0 Hounsfield unit (HU). In the middle of the phantom was a wire (point), and on the outside of the phantom was air with a pixel value of -1000 HU. If the phantom diameter was assumed to be 50 mm, then each pixel had size of  $50 \text{ mm}/512=0.0977 \text{ mm}\approx 0.1 \text{ mm}$ . The wire (point) size was about 0.25 mm. With this size, the spatial resolution of the CT can be detected to the limit of  $1/2d$  or about 2 cycles/mm. This was enough to simulate a real physical phantom for measuring MTF because the spatial resolution of many CT machines is in the range of 0.5-1.5 cycles/mm. In this study, there were three phantoms with three different pixel values of wires, as shown in Figure 1. Figure 1(a) shows phantom with pixel value of 50 HU, Figure 1(b) shows phantom with pixel value of 100 HU, and Figure 1(c) shows phantom with pixel value of 150 HU.

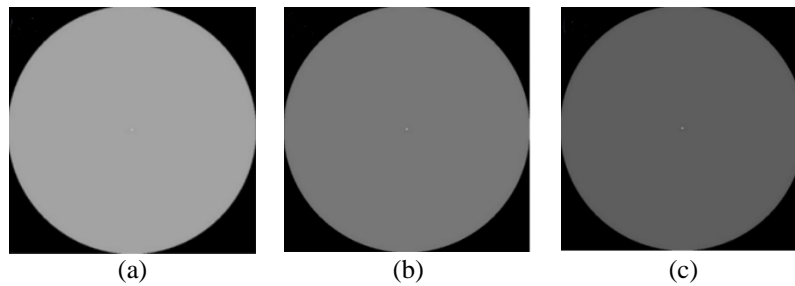


Figure 1. Three computational phantoms developed in this study. Phantoms had a diameter of 512 pixels and mimicked water with a value of 0 HU. In the middle of the phantoms there was a wire (point) for measuring MTF with diameter of 0.25 mm with three different pixel values, i.e. (a) 50 HU, (b) 100 HU, and (c) 150 HU

**2.2. Phantom image degradation and MTF calculation**

The spatial resolutions of the computational phantoms  $P(x,y)$  were degraded by convolution with a point spread function ( $PSF(x,y)$ ), after which various levels of Gaussian noise  $N(x,y)$  were added [33]. The image degradation was modeled by:

$$I(x,y) = \frac{1}{k} [P(x,y) \otimes PSF(x,y)] + N(x,y) \tag{1}$$

image normalization was accomplished by dividing the image by  $k$ , were:

$$k = \text{sum}(\text{sum}(PSF(x,y))) \tag{2}$$

The degradation process can be seen in Figure 2. Each image of a point phantom was blurred by a standard deviation of  $\sigma = 0.031$  mm and various noises added from 0 HU to 25% of the wire (point) pixel value. The noise variation is shown in Table 1. Each measurement was repeated 10 times, and the means and standard deviations of the MTF curves were calculated.

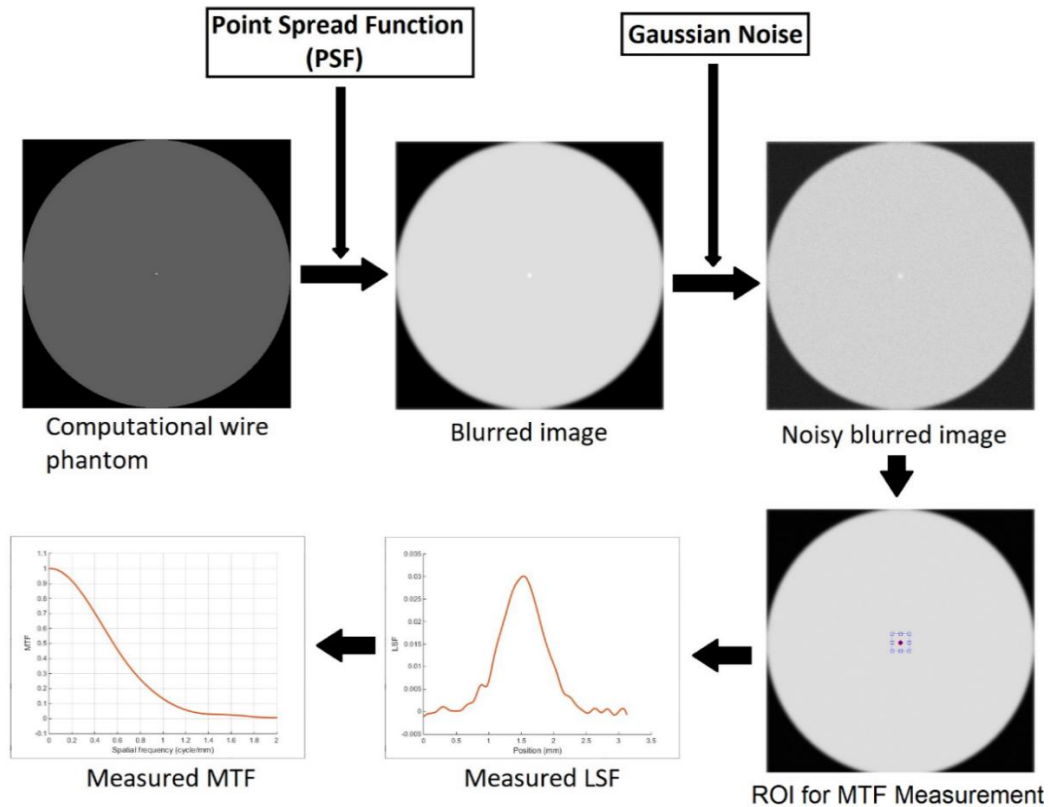


Figure 2. Modeling of spatial resolution and noise on a point phantom, and the MTF measurement process

Table 1. Noise values are given to each computational point phantom

Pixel value of point phantom (HU)	Added noise (HU)					
50	0	2.5	5.0	7.5	10.0	12.5
100	0	5.0	10.0	15.0	20.0	25.0
150	0	7.5	15.0	22.5	30.0	37.5

We used automatic MTF measurement described in previous studies [34], [35]. The first step was to automatically determine the region of interest (ROI). The center of the point image was chosen as the center of ROI with size of  $32 \times 32$  pixels. The profile of pixel values was created from the pixels within the ROI. Both edges of the ROI profile were zeroed by subtracting the mean value of 5 pixels on the left and right of the profile. This profile is the line spread function (LSF), which was then normalized in order to obtain an MTF with value of 1 at a spatial frequency of  $0 \text{ mm}^{-1}$ , after Fourier transformation. The 10% and 50% MTF were calculated.

### 3. RESULTS AND DISCUSSION

#### 3.1. MTF without noise

Blurring is obtained by convolving the phantom image (Figure 1) and the PSF, and the results are shown in Figure 3. There are three phantoms with different point pixel values, i.e. (a) 50 HU, (b) 100 HU, and (c) 150 HU. In Figure 3, the noise in the images is 0 HU. The MTF curves for three point phantoms with pixel variations of 50, 100, and 150 HU are shown in Figure 4. The three MTF curves overlap, indicating that

the MTF curves are identical. This shows that regardless of the contrast between the point object and the background, the MTFs are identical, if there is no added noise. The values of 10% MTF and 50% MTF for the three phantoms are 1.06 cycles/mm and 0.58 cycles/mm, respectively.

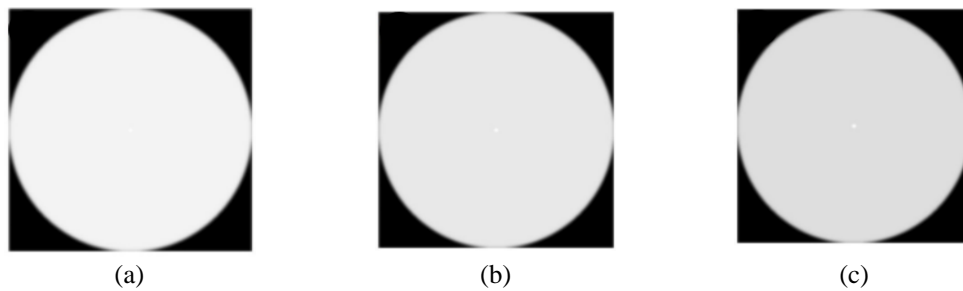


Figure 3. The images of the point phantoms after blurring (second line) used to calculate the MTFs. Pixel values of the point are (a) 50 HU, (b) 100 HU, and (c) 150 HU

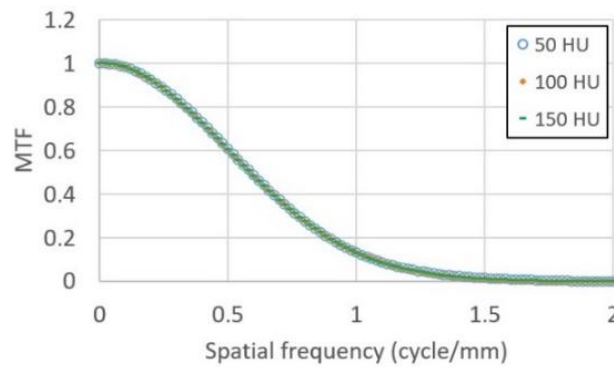


Figure 4. MTF curves of three-point phantoms for pixel values of 50, 100 and 150 HU with noise level of 0 HU. The MTFs of the three phantoms are comparable and overlap each other

**3.2. MTF with noise**

Noise levels from 0 HU to 12.5 HU were added to the point phantom of 50 HU, and the MTFs calculated Figure 5. Greater noise levels make the MTF curves fluctuate more from those without noise. This is also observed in the point phantom of 100 HU Figure 6 and in the point phantom of 150 HU Figure 7. The values of 10% MTF and 50% MTF are shown in Tables 2-4. Tables 3 and 4 shows that the 10% MTF values at the 25% noise reach more than 2.0 cycle/mm.

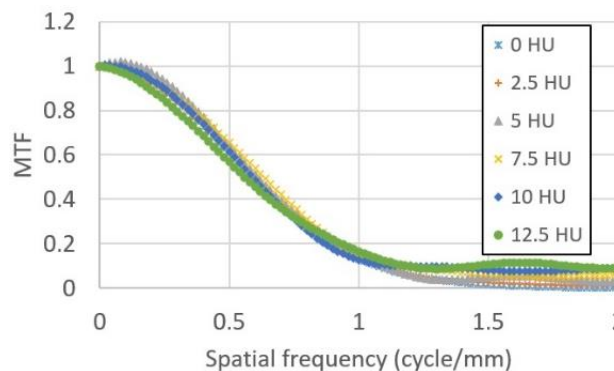


Figure 5. The mean curve of MTFs for the point phantom of 50 HU for noise levels from 0 HU to 12.5 HU

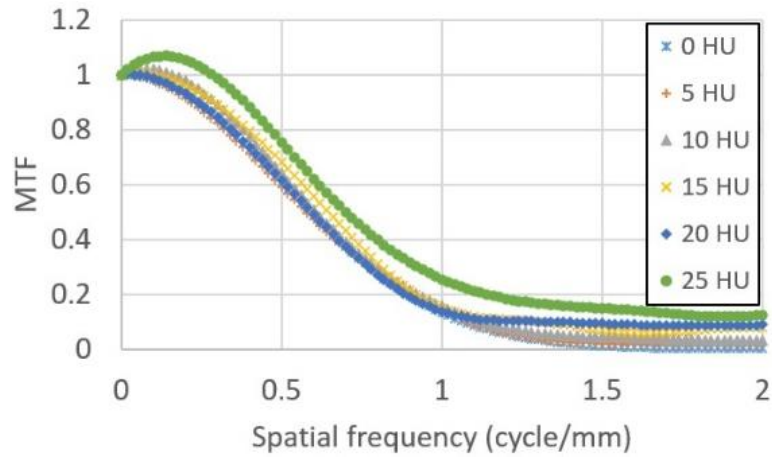


Figure 6. The mean curve of MTF for the point phantom of 100 HU for noise levels from 0 HU to 25 HU

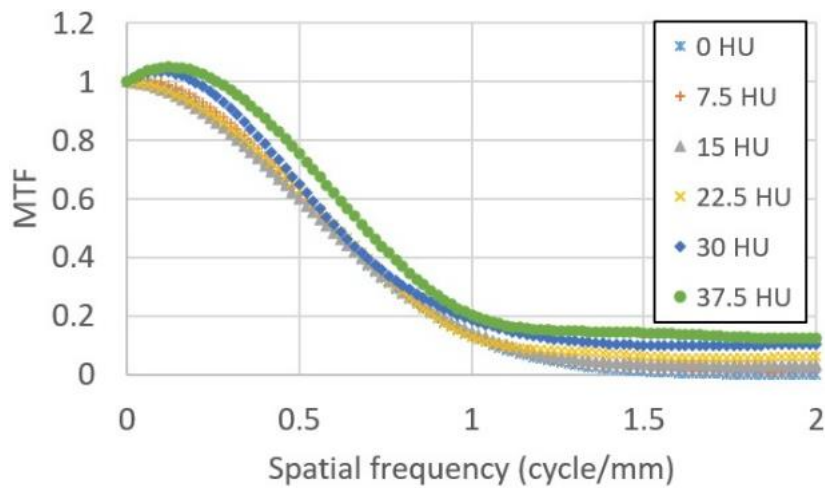


Figure 7. The mean curve of MTFs for the point phantom of 150 HU for noise levels from 0 HU to 37.5 HU

Table 2. The mean values of 10% MTF and 50% MTF for the point phantom of 50 HU and for noise levels from 0 HU to 12.5 HU

Added noise (HU)	10% MTF (cycle/mm)	50% MTF (cycle/mm)
0	1.06	0.58
2.5	1.09	0.59
5.0	1.09	0.60
7.5	1.17	0.63
10.0	1.18	0.58
12.5	1.18	0.55

Table 3. The mean values of 10% MTF and 50% MTF for the point phantom of 100 HU and for noise levels from 0 HU to 25 HU

Added noise (HU)	10% MTF (cycle/mm)	50% MTF (cycle/mm)
0	1.06	0.58
5.0	1.07	0.57
10.0	1.12	0.60
15.0	1.29	0.64
20.0	1.30	0.59
25.0	>2.00	0.69

Table 4. The mean values of 10% MTF and 50% MTF for the point phantom of 150 HU and for noise levels from 0 HU to 37.5 HU

Added noise (HU)	10% MTF (cycle/mm)	50% MTF (cycle/mm)
0	1.06	0.58
7.5	1.07	0.59
15.0	1.10	0.58
22.5	1.09	0.61
30.0	1.58	0.61
37.5	>2.0	0.69

**3.3. Standard deviation of MTF with noise variation**

The curves of mean and standard deviation of MTFs for the point phantom of 50 HU are shown in Figure 8 with noise levels of 0, 2.5, 5, 7.5, 10, and 12.5 HU Figure 8 (a-f). They show that the more noise is added to the point phantom image, the larger standard deviation of the MTF is obtained. This is also shown on the point phantom of 100 HU depicted in Figure 9 with noise levels of 0, 5, 10, 15, 20, and 25 HU Figures 9 (a)-(f), and for the point phantom of 150 HU depicted in Figure 10 with noise levels of 0, 7.5, 15, 22.5, 30, and 37.5 HU Figures 10 (a)-(f). The error bars represent standard deviation and the blue lines are the mean value of MTFs.

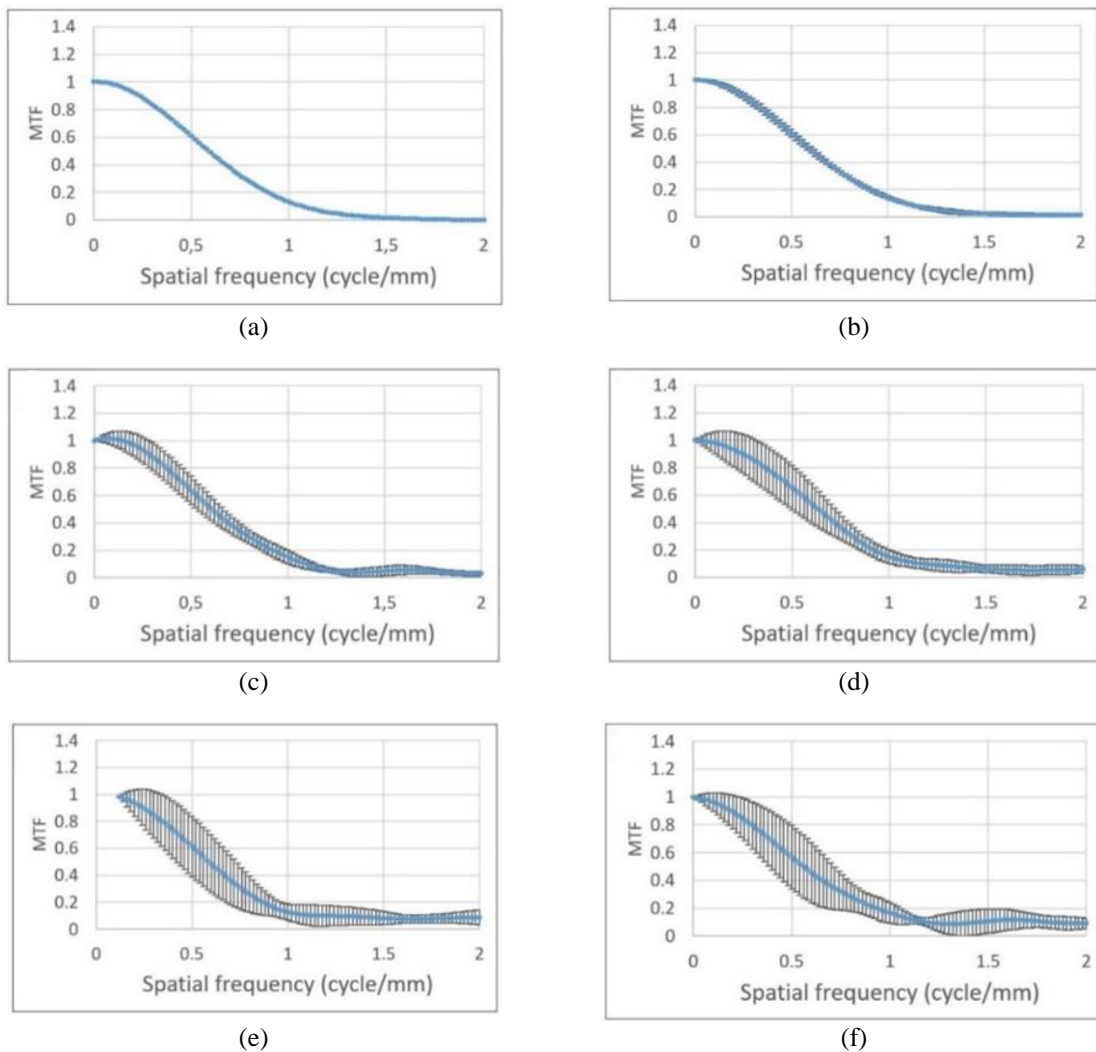


Figure 8. The curves of mean and standard deviation of MTFs for the point phantom of 50 HU and various noises. (a) 0 HU, (b) 2.5 HU, (c) 5 HU, (d) 7.5 HU, (e) 10 HU, and (f) 12.5 HU. Measurements are performed 10 repetitions

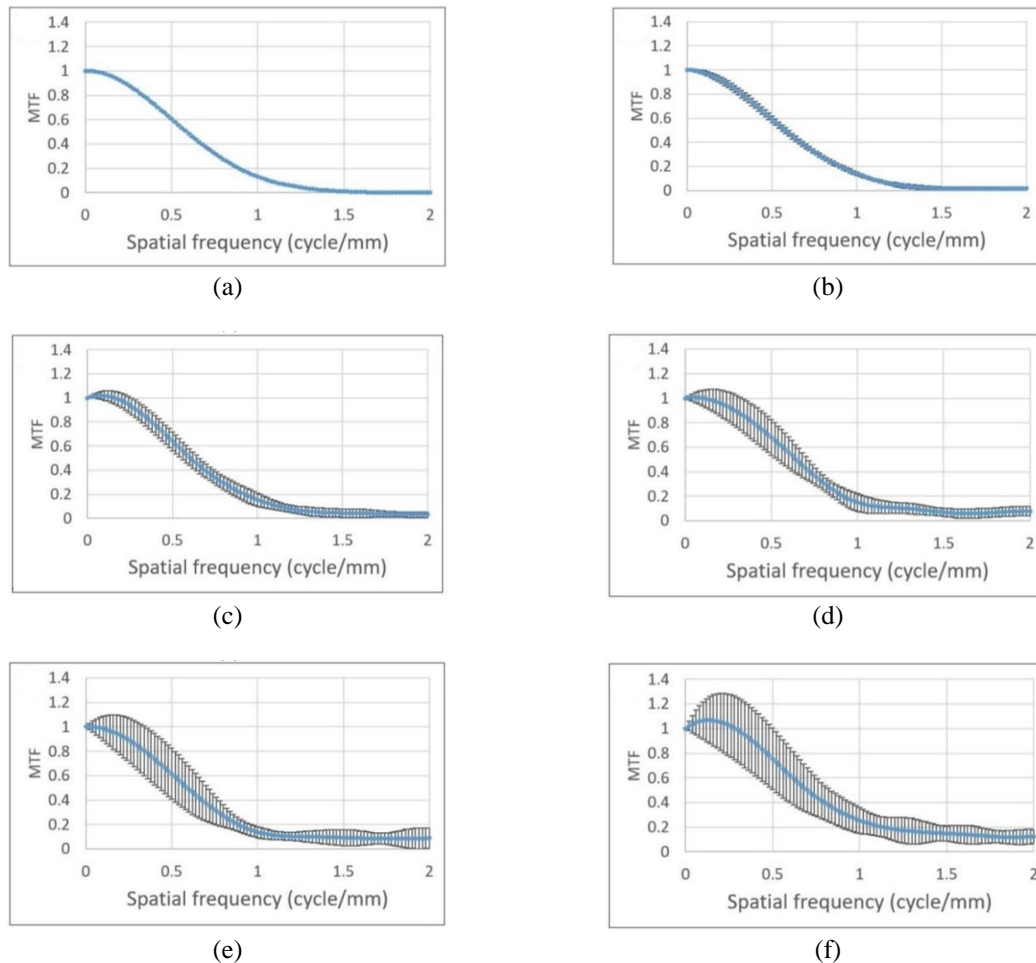


Figure 9. The curves of mean and standard deviation of MTFs for the point phantom of 100 HU and various noises. (a) 0 HU, (b) 5 HU, (c) 10 HU, (d) 15 HU, (e) 20 HU, and (f) 25 HU. Measurements are performed 10 repetitions

Efforts to obtain spatial resolution accurately are very important [26]. The accuracy of the spatial resolution is affected by many things, including the amount of noise in the image. Gonzalez-Lopez developed artificial images using Monte Carlo simulation which were used to simulate the sampling, blurring, and noise processes [28]. Phantoms are used to determine the impact of noise in measuring spatial resolution in images [12]. The phantoms include the bar, edge and star bar phantom. In the current study, point computational phantoms were developed. The phantoms comprised of various compositions with pixel values from 50 HU to 150 HU. Noise up to a quarter of the pixel value of the point was added to the phantoms to evaluate its effect on the MTF value.

If a large amount of noise is added to the phantom image, it caused greater standard deviation of the spatial resolution. This result is consistent with the previous research by Gonzales-Lopez [28] using bar, edge and star bar phantoms. As a result, medical physicists should ensure that noise in the image is small when measuring spatial resolution. In practice, noise levels in the image should not be greater than 10% of the contrast value between a point object and the background. If the noise is greater than 10%, then a fitting technique, such as those proposed Takenaga *et al.* [23] or Mori [32], should be implemented.

The low noise level could be easily achieved by increasing the tube loading (mAs) or radiation dose [21], [31]. The level of radiation does not matter from the dose aspect because the scan is performed on a phantom. However, some CTs have an automatic system, so that increasing the tube loading causes the focal spot to increase so that the spatial resolution will decrease [34].

The advantage of using computational phantom is that the amount of noise can be set at will. However, the drawback is that the modeled noise may not be the same as the actual noise in a CT scanner. Moreover, the use of iterative reconstruction (IR) in CT images results in non-uniform noise. However, the Gaussian noise used in this study can still be used as a reference regarding the effect of the amount of noise

on the accuracy of the MTF value. To create non-uniform noise a circular object with various material types can be used instead of the point phantom. The MTF value should be calculated by taking into account the noise and contrast of the objects simultaneously. This is called as the task transfer function (TTF) [35]. Development of a computational phantom for TTF evaluation will be carried out in a future study.

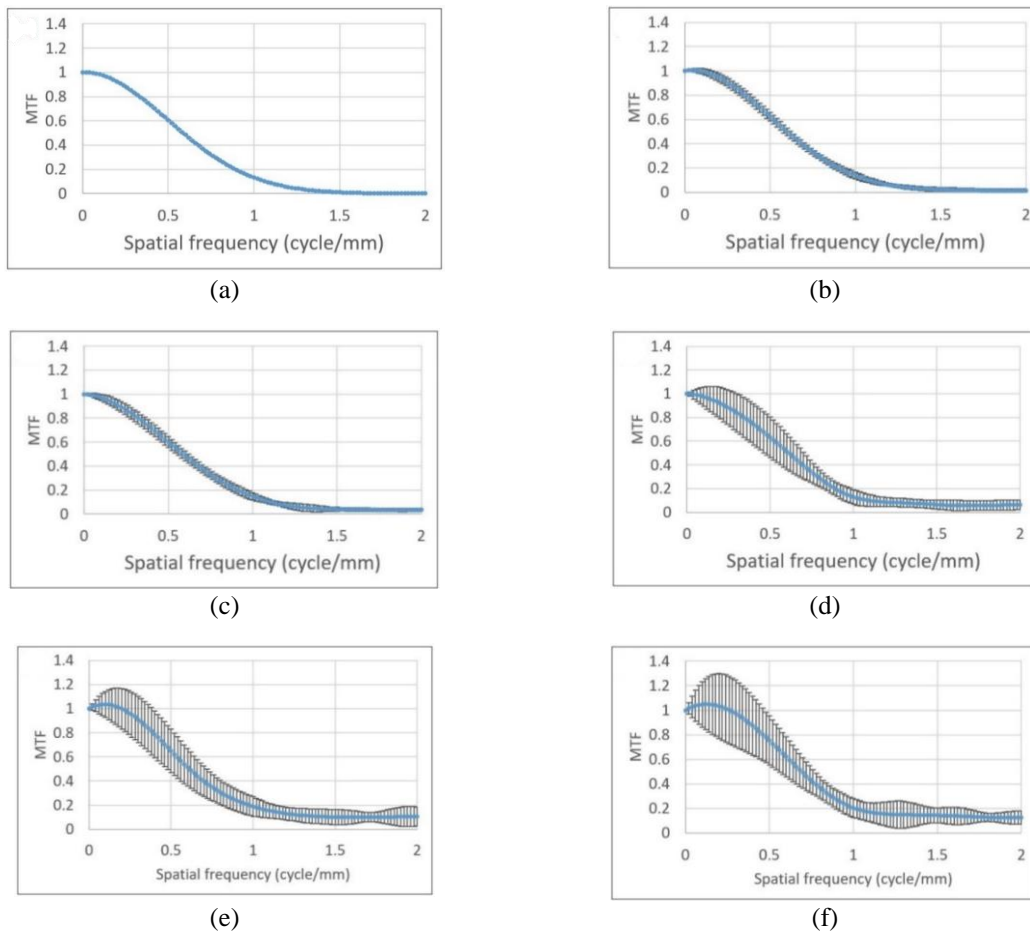


Figure 10. The curves of mean and standard deviation of MTFs for the point phantom of 150 HU and various noises. (a) 0 HU, (b) 7.5 HU, (c) 15 HU, (d) 22.5 HU, (e) 30 HU, and (f) 37.5 HU. Measurements are performed 10 repetitions

#### 4. CONCLUSION

We successfully developed computational phantoms to evaluate the effect of noise on the MTF. By using computational phantoms, the value of the spatial resolution and the amount of noise can be determined independently. The results show that the amount of noise affects the accuracy of the MTF. We found that for a noise value of 10% of the image contrast, the results in a significantly different MTF curve from the actual value.

#### ACKNOWLEDGEMENTS

This study was funded by the World Class Research University (WCRU), Diponegoro University, Contract number: 118-11/UN7.6.1/PP/2021.

#### REFERENCES

- [1] C. Anam, F. Haryanto, R. Widita, I. Arif, and G. Dougherty, "An investigation of spatial resolution and noise in reconstructed CT images using iterative reconstruction (IR) and filtered back-projection (FBP)," *J. Phys. Conf. Ser.*, vol. 1127, p. 012016, Jan. 2019, doi: 10.1088/1742-6596/1127/1/012016.
- [2] R. Padgett and C. J. Kotre, "Development and application of programs to measure modulation transfer function, noise power spectrum and detective quantum efficiency," *Radiat. Prot. Dosimetry*, vol. 117, no. 1–3, pp. 283–287, Dec. 2005, doi: 10.1093/rpd/nci740.






- [3] A. M. A. Roa, H. K. Andersen, and A. C. T. Martinsen, "CT image quality over time: comparison of image quality for six different CT scanners over a six-year period," *J. Appl. Clin. Med. Phys.*, vol. 16, no. 2, pp. 350–365, Mar. 2015, doi: 10.1120/jacmp.v16i2.4972.
- [4] G. Dougherty and Z. Kawaf, "The point spread function revisited: image restoration using 2-D deconvolution," *Radiography*, vol. 7, no. 4, pp. 255–262, Nov. 2001, doi: 10.1053/radi.2001.0341.
- [5] N. J. Schneiders and S. C. Bushong, "Computer assisted MTF determination in CT," *Med. Phys.*, vol. 7, no. 1, pp. 76–78, Jan. 1980, doi: 10.1118/1.594769.
- [6] C. Anam, T. Fujibuchi, W. S. Budi, F. Haryanto, and G. Dougherty, "An algorithm for automated modulation transfer function measurement using an edge of a PMMA phantom: Impact of field of view on spatial resolution of CT images," *J. Appl. Clin. Med. Phys.*, vol. 19, no. 6, pp. 244–252, Nov. 2018, doi: 10.1002/acm2.12476.
- [7] E. Zabilal Hak, C. Anam, W. Setia Budi, and G. Dougherty, "An improvement in automatic MTF measurement in CT images using an edge of the PMMA phantom," *J. Phys. Conf. Ser.*, vol. 1505, no. 1, p. 012039, Mar. 2020, doi: 10.1088/1742-6596/1505/1/012039.
- [8] F. Mievville, S. Beaumont, T. Torfeh, F. Gudinchet, and F. R. Verdun, "Computed tomography commissioning programmes: how to obtain a reliable MTF with an automatic approach?," *Radiat. Prot. Dosimetry*, vol. 139, no. 1–3, pp. 443–448, Apr. 2010, doi: 10.1093/rpd/ncq050.
- [9] E. L. Nickoloff and R. Riley, "A simplified approach for modulation transfer function determinations in computed tomography," *Med. Phys.*, vol. 12, no. 4, pp. 437–442, Jul. 1985, doi: 10.1118/1.595706.
- [10] R. T. Droege and R. L. Morin, "A practical method to measure the MTF of CT scanners," *Med. Phys.*, vol. 9, no. 5, pp. 758–760, Sep. 1982, doi: 10.1118/1.595124.
- [11] M. Ohkubo, S. Wada, T. Matsumoto, and K. Nishizawa, "An effective method to verify line and point spread functions measured in computed tomography," *Med. Phys.*, vol. 33, no. 8, pp. 2757–2764, Jul. 2006, doi: 10.1118/1.2214168.
- [12] J. Sanders, L. Hurwitz, and E. Samei, "Patient-specific quantification of image quality: An automated method for measuring spatial resolution in clinical CT images," *Med. Phys.*, vol. 43, no. 10, pp. 5330–5338, Sep. 2016, doi: 10.1118/1.4961984.
- [13] C. Anam, W. Budi, T. Fujibuchi, F. Haryanto, and G. Dougherty, "Validation of the tail replacement method in MTF calculations using the homogeneous and non-homogeneous edges of a phantom," *J. Phys. Conf. Ser.*, vol. 1248, no. 1, p. 012001, Jun. 2019, doi: 10.1088/1742-6596/1248/1/012001.
- [14] M. Kachelrieß and W. A. Kalender, "Presampling, algorithm factors, and noise: Considerations for CT in particular and for medical imaging in general," *Med. Phys.*, vol. 32, no. 5, pp. 1321–1334, Apr. 2005, doi: 10.1118/1.1897083.
- [15] T. G. Flohr, K. Stierstorfer, S. Ulzheimer, H. Bruder, A. N. Primak, and C. H. McCollough, "Image reconstruction and image quality evaluation for a 64-slice CT scanner with z-flying focal spot," *Med. Phys.*, vol. 32, no. 8, pp. 2536–2547, Jul. 2005, doi: 10.1118/1.1949787.
- [16] W. A. Kalender and A. Polacin, "Physical performance characteristics of spiral CT scanning," *Med. Phys.*, vol. 18, no. 5, pp. 910–915, Sep. 1991, doi: 10.1118/1.596607.
- [17] S. Mori *et al.*, "Physical performance evaluation of a 256-slice CT-scanner for four-dimensional imaging," *Med. Phys.*, vol. 31, no. 6, pp. 1348–1356, May 2004, doi: 10.1118/1.1747758.
- [18] H. Arabi, A. R. Kamali Asl, M. R. Ay, and H. Zaidi, "Monte Carlo-based assessment of the trade-off between spatial resolution, field-of-view and scattered radiation in the variable resolution X-ray CT scanner," *Phys. Medica*, vol. 31, no. 5, pp. 510–516, Jul. 2015, doi: 10.1016/j.ejmp.2015.03.014.
- [19] K. Li, J. Garrett, Y. Ge, and G.-H. Chen, "Statistical model based iterative reconstruction (MBIR) in clinical CT systems. Part II. Experimental assessment of spatial resolution performance," *Med. Phys.*, vol. 41, no. 7, p. 071911, Jun. 2014, doi: 10.1118/1.4884038.
- [20] H. Arabi, A. R. K. Asl, and S. M. Aghamiri, "The effect of focal spot size on the spatial resolution of variable resolution X-ray CT scanner," *Iran. J. Radiat. Res.*, vol. 8, no. 1, pp. 37–43, 2010.
- [21] G. Dougherty and D. Newman, "Measurement of thickness and density of thin structures by computed tomography: A simulation study," *Med. Phys.*, vol. 26, no. 7, pp. 1341–1348, Jul. 1999, doi: 10.1118/1.598629.
- [22] S. Prevrhal, J. C. Fox, J. A. Shepherd, and H. K. Genant, "Accuracy of CT-based thickness measurement of thin structures: Modeling of limited spatial resolution in all three dimensions," *Med. Phys.*, vol. 30, no. 1, pp. 1–8, Dec. 2002, doi: 10.1118/1.1521940.
- [23] T. Takenaga, S. Katsuragawa, M. Goto, M. Hatemura, Y. Uchiyama, and J. Shiraishi, "Modulation transfer function measurement of CT images by use of a circular edge method with a logistic curve-fitting technique," *Radiol. Phys. Technol.*, vol. 8, no. 1, pp. 53–59, Jan. 2015, doi: 10.1007/s12194-014-0286-x.
- [24] J. M. Boone and J. A. Seibert, "An analytical edge spread function model for computer fitting and subsequent calculation of the LSF and MTF," *Med. Phys.*, vol. 21, no. 10, pp. 1541–1545, Oct. 1994, doi: 10.1118/1.597264.
- [25] J. Garayoa and P. Castro, "A study on image quality provided by a kilovoltage cone-beam computed tomography," *J. Appl. Clin. Med. Phys.*, vol. 14, no. 1, pp. 239–257, Jan. 2013, doi: 10.1120/jacmp.v14i1.3888.
- [26] J. H. Siewerdsen, I. A. Cunningham, and D. A. Jaffray, "A framework for noise-power spectrum analysis of multidimensional images," *Med. Phys.*, vol. 29, no. 11, pp. 2655–2671, Oct. 2002, doi: 10.1118/1.1513158.
- [27] H. R. Choi, R. E. Kim, C. W. Heo, C. W. Kim, M. S. Yoo, and Y. Lee, "Optimization of dose and image quality using self-produced phantom with various diameters in pediatric abdominal CT scan," *Optik (Stuttg.)*, vol. 168, pp. 54–60, Sep. 2018, doi: 10.1016/j.ijleo.2018.04.066.
- [28] A. González-López, "Effect of noise on MTF calculations using different phantoms," *Med. Phys.*, vol. 45, no. 5, pp. 1889–1898, May 2018, doi: 10.1002/mp.12847.
- [29] C. H. McCollough *et al.*, "The phantom portion of the American College of Radiology (ACR) computed tomography (CT) accreditation program: practical tips, artifact examples, and pitfalls to avoid," *Med. Phys.*, vol. 31, no. 9, pp. 2423–2442, Aug. 2004, doi: 10.1118/1.1769632.
- [30] W. A. Kalender, "Dose in x-ray computed tomography," *Phys. Med. Biol.*, vol. 59, no. 3, pp. R129–R150, Feb. 2014, doi: 10.1088/0031-9155/59/3/R129.
- [31] I. Mori and Y. Machida, "Deriving the modulation transfer function of CT from extremely noisy edge profiles," *Radiol. Phys. Technol.*, vol. 2, no. 1, pp. 22–32, Jan. 2009, doi: 10.1007/s12194-008-0039-9.
- [32] S. Richard, D. B. Husarik, G. Yadava, S. N. Murphy, and E. Samei, "Towards task-based assessment of CT performance: System and object MTF across different reconstruction algorithms," *Med. Phys.*, vol. 39, no. 7Part1, pp. 4115–4122, Jun. 2012, doi: 10.1118/1.4725171.




- [33] C. Anam *et al.*, "Development of a computational phantom for validation of automated noise measurement in CT images," *Biomed. Phys. Eng. Express*, vol. 6, no. 6, p. 065001, Nov. 2020, doi: 10.1088/2057-1976/abb2f8.
- [34] C. Anam *et al.*, "Automated MTF measurement in CT images with a simple wire phantom," *Polish J. Med. Phys. Eng.*, vol. 25, no. 3, pp. 179–187, Sep. 2019, doi: 10.2478/pjmpe-2019-0024.
- [35] E. Samei *et al.*, "Performance evaluation of computed tomography systems: summary of AAPM task group 233," *Med. Phys.*, vol. 46, no. 11, Nov. 2019, doi: 10.1002/mp.13763.

## BIOGRAPHIES OF AUTHORS






**Dr. Choirul Anam**    completed his Ph.D in Physics Department, Bandung Institute of Technology (ITB). He received Master degree from University of Indonesia (UI) and the B.Sc degree from Diponegoro University (UNDIP). He is currently working as a Lecturer and Researcher at the UNDIP. His research interests are medical image processing and dosimetry for diagnostic radiology, particularly in CT. He has authored and co-authored over 150 papers. One of his papers published in the Journal of Applied Clinical Medical Physics (JACMP) had been awarded as the Best Medical Imaging Physics Article in 2016. He received the Best Paper Award during 15th South East Asian Congress of Medical Physics (SEACOMP). He was also recognised as an Outstanding Reviewer for the Physics in Medicine and Biology (PMB) in 2018 and for the Biomedical Physics and Engineering Express (BPEX) in 2019. He was also awarded as the SEAFOMP Young Leader Awards 2019 for his contribution in CT dosimetry and image quality from the South East Asian Federation of Organizations for Medical Physics (SEAFOMP). He is developer of two software, i.e. IndoseCT (for calculating and managing radiation dose of CT) and IndoQCT (for measuring CT image quality). He can be contacted at email: [anam@fisika.fsm.undip.ac.id](mailto:anam@fisika.fsm.undip.ac.id).






**Ariij Naufal**    is a graduate student of the physics master's program at Diponegoro University. Together with Dr. Choirul Anam, he developed IndoQCT. He can be contacted by email: [ariij.2019@fisika.fsm.undip.ac.id](mailto:ariij.2019@fisika.fsm.undip.ac.id).



**Prof. Heri Sutanto**    is a lecturer in materials physics at Diponegoro University. His expertise is thin films, nanomaterials, and medical materials. He can be contacted at email: [herisutanto@live.undip.ac.id](mailto:herisutanto@live.undip.ac.id).



**Prof. Geoff Dougherty**    graduated with First Class in Physics at Manchester University, did a post-baccalaureate teaching certificate at Leeds University, taught at a community college and then completed a Ph.D on DNA-drug interactions at Keele University. This was followed by a post-doc period investigating closed-circular DNA at the Swiss Federal Institute of Technology, Zurich. He taught at the Science University of Malaysia; did research on DNA-drug binding using electron spin resonance at Monash University, Australia; and taught at the University of the South Pacific, Fiji and Oxford Brookes University. After that he moved to Kuwait as Professor of Radiologic Sciences (1992-2002). He moved to California in 2002, where he is currently Professor of Applied Physics and Medical Imaging. He applies image analysis and pattern recognition techniques to medical images from a variety of modalities in an effort to extract the maximum quantifiable diagnostic and prognostic information from them. His three Fulbright experiences (two as Senior Scholar and one as a Specialist) have resulted in many new collaborations. He can be contacted at email: [Geoff.Dougherty@csuci.edu](mailto:Geoff.Dougherty@csuci.edu)